Kinetic Studies of Thermally Induced Phase Separation in Polymer–Diluent System

HIDETO MATSUYAMA, SYUNSUKE KUDARI, HISAYA KIYOFUJI, YOSHIRO KITAMURA

Department of Environmental Chemistry and Materials, Okayama University,
2-1-1 Tsushima-naka, Okayama 700-8530, Japan

Received 22 April 1999; accepted 2 September 1999

ABSTRACT: Thermally induced phase separation was studied by the light scattering in polypropylene/methyl salicylate system. Data could be well fitted with the linear Cahn theory for spinodal decomposition (SD) in the early stage of phase separation. Characteristic properties of the early stage of SD, such as an apparent diffusion coefficient and an interphase periodic distance, were obtained. The periodic distance ranged from 3 μm to 4 μm. The growth of the phase-separated structure obeyed power-law scaling in the later stage, and the structure factor could be scaled into a universal time-independent form. Domain sizes obtained from the light-scattering measurements were consistent with the optical microscope measurements. © 2000 John Wiley & Sons, Inc. J Appl Polym Sci 76: 1028–1036, 2000

Key words: thermally induced phase separation; light scattering; spinodal decomposition; structure factor; droplet growth

INTRODUCTION

The thermally induced phase separation (TIPS) process is one of the most popular ways of making microporous membranes.[1,2] In this process, a polymer is dissolved in a diluent at an elevated temperature, and by cooling or quenching the solution, phase separation is induced. The general type of the phase separation is a liquid–liquid phase separation, where the solution separates into a polymer-rich continuous phase and a polymer-lean droplet phase. After the phase separation is induced, the diluent is removed by extraction, evaporation, or freeze drying. The polymer-lean phase finally becomes a pore of the resultant membrane. A large number of microporous membranes have been prepared by TIPS process from various polymers, such as polypropylene, polyethylene, poly(vinylidene fluoride), poly(methyl methacrylate), and so on.[3–23]

In the preparation of microporous membrane by TIPS process, clarification of kinetics of the phase separation is essential to control and design the pore size and the porosity. Kinetics of droplet growth in the later stage of the liquid–liquid TIPS have been widely investigated.[24–33] McGuire et al. reviewed them briefly.[33] The domain size S was measured by optical microscopy,[25,33] light scattering,[24,26,28,29] and electron microscopy.[27,30,31,32] S was generally correlated to the time t with a scaling relation as follows:

$$S \propto t^{\lambda} \tag{1}$$

where λ is a scaling exponent. Several models for the droplet growth were presented with the different λ values.[34] Both coalescence and Ostwald ripening mechanism can predict $\frac{1}{3}$ for λ; whereas, λ is unity for the hydrodynamic flow mechanism. Song and Torkelson found the time-dependency of

Correspondence to: H. Matsuyama, Department of Chemistry and Materials Technology, Kyoto Institute of Technology, Matsugasaki, Sakyo-ku, Kyoto 606-8585, Japan (matuyama@chem.kit.ac.jp).

Journal of Applied Polymer Science, Vol. 76, 1028–1036 (2000)

the scaling exponent.[30,32] At relatively sort coarsening times, the droplet growth rate had an exponent of $\frac{1}{3}$ in agreement with the theories by Ostwald ripening or coalescence mechanisms. There was a crossover to a much faster growth rate yielding an exponent of 1.0 at larger coarsening times. McGuire et al. proposed a coalescence-induced coalescence mechanism.[35] In this mechanism, forces created as a result of a coalescence event cause a flow of the matrix fluid, which then impacts nearby droplets and causes more coalescence. They reported that good quantitative agreement was found between the model and the experimental droplet growth data in polypropylene/diphenyl ether system.

In contrast to a number of studies on kinetics of the droplet growth, there have been reported a few studies on the phase separation at the early stage in polymer–diluent systems. Aartsen and Smolders investigated the liquid–liquid phase separation in poly(2,6-dimethyl-1,4-phenylene ether)/caprolactam system.[36] It was found by the light-scattering measurements that the phase separation took place via a spinodal decomposition (SD) mechanism. Kuwahara and Kubota investigated the spinodal decomposition in a critical mixture of polydimethylsiloxane/diethyl carbonate system by a time-resolved light-scattering technique, focusing especially on the early and intermediate stages of phase separation.[37] They showed that the early stage of SD predicted by the linear Cahn theory[38] was clearly observed and the linearized theory worked very well. Kinetics of SD in polystyrene/cyclohexane system was studied by Lal and Bansil.[28] The early stage of the phase separation process showed an exponential increase in intensity. An analysis in terms of the linear Cahn theory was made to determine the extrapolated growth rate at zero time and hence the initial diffusion constant.

In this paper, we investigate both the early and later stages of TIPS process in polypropylene/methyl salicylate system by the light-scattering measurements. Polypropylene was used, because it is a popular polymer in preparing the microporous membrane by TIPS process.

EXPERIMENTAL

Materials

Isotactic polypropylene (iPP, Aldrich Chemical Inc., M_w = 250000) and methyl salicylate (MS, Nacalai Tesque Co.) were used as polymer and diluent without further purification. Homogeneous polymer–diluent solid sample was prepared by the method previously described.[12]

Phase Diagram

Cloud point curve for iPP/MS system was determined as follows. The homogeneous polymer–diluent sample was chopped into small pieces and placed between a pair of microscope cover slips. A Teflon film of 97 μm thickness with a square opening was inserted between the cover slips. The sample was heated on a hot stage (Linkam, LK-600PH) at 150°C for 3 min to assure homogeneity. Then it was cooled to 25°C at a controlled rate of 10°C/min. The temperature of the stage was manipulated by a Linkam L-600A controller. Cloud points were determined visually by noting the appearance of turbidity under an optical microscope (Olympus, BX50).

A DSC (Perkin–Elmer DSC-7) was used to determine the dynamic crystallization temperature T_c. The solid sample was sealed in an aluminum DSC pan, melted at 200°C for 3 min and then cooled at a 10°C/min to 25°C. The onset of the exothermic peak during the cooling was taken as the crystalline temperature.

Light-Scattering Measurements

The light-scattering measurement was carried out with a polymer dynamics analyzer (Otsuka Electronics Co., DYNA-3000). A He-Ne laser (5 mW) was used as a light source. Between the light source and the sample, a neutral density filter and a polarizer were set. The light scattered by the sample passed through an analyzer and was detected by a CCD camera. An exposure time was 0.4 s, and the light scattering was measured with time intervals of about 1 s and 10 s for the measurements of the early and the later stages of phase separation, respectively.

For the measurements, the hot stage was located between the laser and the detector. The sample sealed with two cover slips was placed on the stage and was heated at 150°C for 1 min. Then, it was quenched to the desired temperature at the cooling rate of 130°C/min. Temperature difference between the hot stage and the sample was assumed not to be so large in this rapid cooling rate, because the sample thickness was as thin as less than 100 μm. The light scattering was measured after the temperature reached to the desired one.

Droplet Growth Kinetic Studies

The hot stage was placed on the platform of the optical microscope. The image from the microscope was converted to a video signal. The video signal was passed through a video timer and into a videocassette recorder, where it was captured on a videotape for subsequent analysis. To measure the droplet size of the polymer-lean phase, an image analysis was used. The image analysis software package used was Win ROOF (Mitani Co.).

RESULTS AND DISCUSSION

Phase Diagram

Cloud points obtained are shown in Figure 1. As a first approximation, the cloud point curve was assumed to be a coexistence curve.[39] According to Flory's theory in polymer–diluent system, polymer volume fractions of two coexisting phases are given by[39,40]:

$$[(\phi_2^\beta)^2 - (\phi_2^\alpha)^2]\,\chi = \ln\left(\frac{1-\phi_2^\alpha}{1-\phi_2^\beta}\right) + \left(1-\frac{1}{r}\right)(\phi_2^\alpha - \phi_2^\beta) \quad (2)$$

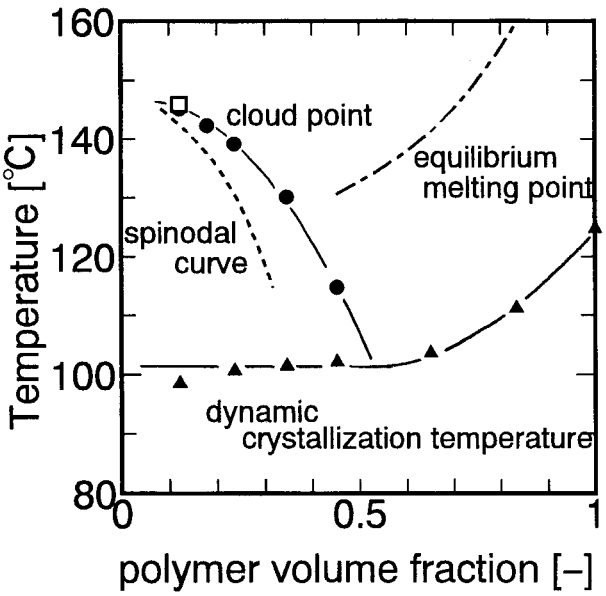

Figure 1 Phase diagram of iPP/MS system: (●) cloud point; (▲) dynamic crystallization temperature; (□) spinodal temperature determined from the light-scattering experiment; (- - - -) calculated spinodal curve; (— - —) calculated equilibrium melting point.

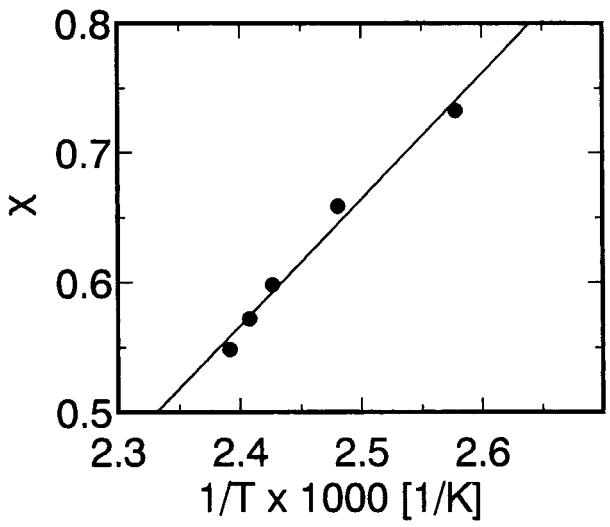

Figure 2 Temperature dependence of the interaction parameter.

$$r[(1-\phi_2^\beta)^2 - (1-\phi_2^\alpha)^2]\,\chi = \ln\left(\frac{\phi_2^\alpha}{\phi_2^\beta}\right) + (r-1)(\phi_2^\alpha - \phi_2^\beta) \quad (3)$$

where ϕ_2^α and ϕ_2^β are the polymer volume fractions in phase α and β, respectively, χ is the interaction parameter, and r is the ratio of the polymer molar volume to the diluent molar volume. The value of r was estimated to be 2030 from M_w of polymer. By simultaneously solving eqs. (2) and (3) with ϕ_2^β shown in Figure 1, χ was determined as a function of temperature. The relation between χ and the reciprocal of temperature $1/T$ is shown in Figure 2. The linear relationship of $\chi = -1.77 + 973/T$ was obtained.

Flory's theory gives the following equation for spinodal.

$$\frac{1}{\nu_1(1-\phi_2)} + \frac{1}{\nu_2\phi_2} - \frac{2\chi}{\nu_1} = 0 \quad (4)$$

Here, ν is the molar volume, and subscripts 1 and 2 denote diluent and polymer, respectively. The spinodal line calculated from eq. (4) with the known χ parameter is shown in Figure 1 as a dotted line. The polymer volume fraction at the critical point ϕ_2^c is given by:

$$\phi_2^c = 1/[1 + (\nu_2/\nu_1)^{1/2}] \quad (5)$$

The determined ϕ_2^c was 0.022. Because the binodal contacts with the spinodal at the critical

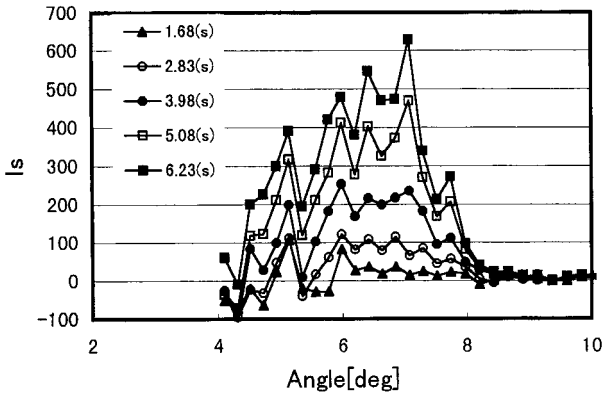

Figure 3 Relation between the scattered intensity and the scattered angle: quench temperature 140.9°C; polymer volume fraction 0.121.

point, a metastable region between the binodal and the spinodal becomes narrow with decreasing the polymer volume fraction to 0.022, as shown in Figure 1.

The dynamic crystallization temperature was shown as symbol ▲ in Figure 1. The crystallization temperature decreased with decreasing the polymer volume fraction and became nearly constant beneath the liquid–liquid region. This tendency is in accordance with that in iPP/n,n-bis(2-hydroxyethyl) tallowamine system.[11] The equilibrium melting point equation is expressed as[39,41]:

$$\frac{1}{T_m} = \left[1 + \frac{R\beta}{\Delta H_u}(1-\phi_2)^2\right]^{-1}\left\{\frac{1}{T_m^0} + \frac{R}{\Delta H_u} \times \left[\left(1-\frac{1}{r}\right)(1-\phi_2) - \frac{\ln \phi_2}{r} - \alpha(1-\phi_2)^2\right]\right\} \quad (6)$$

where T_m and T_m^0 are the melting point of the diluted polymer and the pure polymer, respectively, R is the gas constant, and ΔH_u is the heat of fusion per mole of repeat unit. α and β are the coefficients of temperature dependence of $\chi = \alpha + \beta/T$, as described above. By taking 185°C[42] and 10.1 kJ/mol[43] as T_m^0 and ΔH_u, the equilibrium melting point was calculated. The equilibrium melting point curve is shown in Figure 1 as a dashed line. The dynamic crystallization temperature was fairly lower than the equilibrium melting point because a supercooling is necessary for the actual crystallization of the polymer from solution.[11]

Early Stage of Phase Separation

An example of the light-scattering measurement up to about 6 s after quenching is shown in Figure 3. This was the result when the sample was quenched to 140.9°C. Measurement time shown in this figure corresponds to the elapse of time after temperature reached to the desired value. Therefore, this time does not include time required for quenching. Clear maxima of the scattered light intensity I_s were recognized at the scattered angle θ of about 7°. As time proceeds, the scattered intensity increased with the position of the maximum of I_s unchanged. This result clearly shows that the phase separation in this time scale was at the early stage of SD.

According to the linear Cahn theory[38] in the early stage of SD, I_s can be related with time t as:

$$I_s(q, t) \propto \exp[2R(q)t] \quad (7)$$

where, $R(q)$ is a growth rate of the concentration fluctuation. Wavenumber q is given by eq. (8).

$$q = (4\pi n/\lambda_0)\sin(\theta/2) \quad (8)$$

Here, n is the solution refractive index, and λ is the wavelength of light in vacuo. $R(q)$ can be correlated to q as[28,44]:

$$R(q) = D_{\text{app}}q^2[1 - q^2/(2q_m^2)] \quad (9)$$

where D_{app} is the apparent diffusion coefficient, and q_m is the wavenumber of maximum scattered light intensity. The relation between q_m and the average interphase periodic distance Λ_m is given as follows.

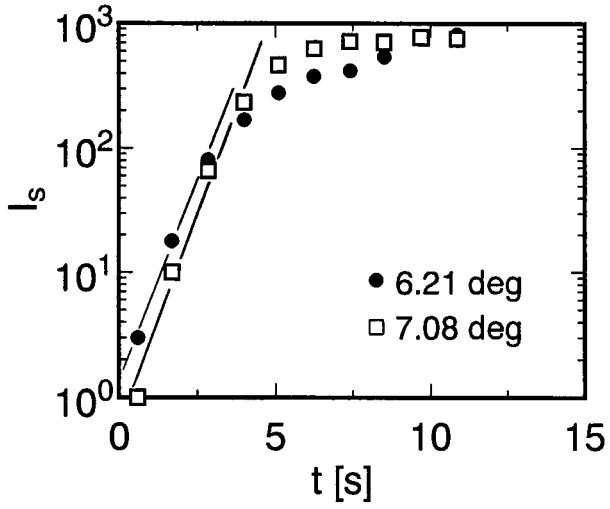

Figure 4 Semilogarithmic plots of I_s against time for the data in Figure 3.

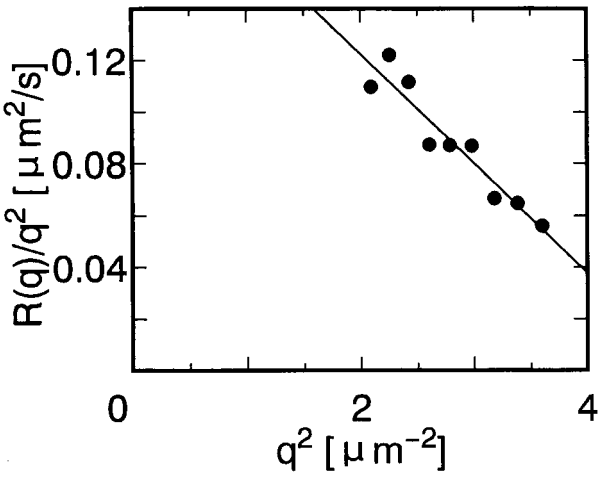

Figure 5 Relation between $R(q)/q^2$ and q^2.

$$q_m = 2\pi/\Lambda_m \tag{10}$$

From eq. (9), we can expect that the plot of $R(q)/q^2$ versus q^2 is linear in the early stage of SD. The intercept of the straight line gives D_{app}, and the slope gives q_m. q_m can be also determined from the direct measurement of I_s versus θ. Semilogarithmic plot of I_s versus t for the data of Figure 3 is shown in Figure 4. The initial growth seems to be exponential, suggesting that the Cahn theory is applicable. Figure 5 shows the plot of $R(q)/q^2$ versus q^2. The obtained linear relation is in accordance with the expectation of eq. (9). Similar linear relations were also obtained when samples were quenched to temperatures of 142.9, 141.9, and 139.9°C.

Characteristic properties of phase separation in the early stage of SD are summarized in Table I. D_{app}, which was determined from the plot of $R(q)/q^2$ versus q^2, increased with the decrease of temperature; that is, with the increase of quench depth. q_m directly determined from the plot of I_s versus θ increased with the increase of quench depth. These value of q_m are roughly in agreement with those determined from the plot of $R(q)/q^2$ versus q^2, as shown in Table I. The characteristic time of the phase separation process, $\tau_0 = 1/(D_{app}q_m^2)$ decreased as quench depth increased. The interphase periodic distance Λ_m ranged from 3 μm to 4 μm. These tendencies in D_{app}, q_m and τ_0 are the same as those reported in polystyrene/cyclohexane system.[28] In the content of mean-field approximation, D_{app} and q_m are given in polymer blend system by[44,45]:

$$D_{app} = D_c(\chi - \chi_s)/\chi_s \tag{11}$$

$$q_m = [18(\chi - \chi_s)/\chi_s]^{1/2}/R_0 \tag{12}$$

where D_c is the translational diffusion coefficient of molecules, χ_s is the Flory–Huggins interaction parameters at spinodal point, and R_0 is the unperturbed end-to-end distance of polymer coil. D_{app} is influenced by both kinetic property of D_c and the thermodynamic property of $(\chi - \chi_s)/\chi_s$). As temperature decreases, D_c decreases because of the increase of the solution viscosity. On the other hand, $(\chi - \chi_s)/\chi_s$ increases with decreasing the temperature. If the latter effect is predominant, D_{app} increases with the decrease of temperature, as shown in Table I. Similarly, the increase of $(\chi - \chi_s)/\chi_s$ with the decrease of temperature leads to the increase of q_m.

D_{app} is plotted against the temperature in Figure 6. The spinodal temperature at which the apparent diffusion coefficient equals zero can be determined from the intersection of the extrapolated diffusion coefficient and the abscissa.[44,46,47] The determined spinodal temperature is 145.9°C and is plotted in Figure 1 as symbol □. This spinodal temperature was close to the binodal curve. The calculated spinodal curve also ap-

Table I Characteristic Properties of Phase Separation in the Early Stage of SD

Temperature (°C)	D_{app} ($\mu m^2/s$)	q_m (μm^{-1})[a]	q_m (μm^{-1})[b]	τ_0 (s)	Λ_m (μm)[c]
142.9	0.131	1.68	1.53	2.70	3.74
141.9	0.166	1.78	1.63	1.90	3.53
140.9	0.207	1.84	1.56	1.43	3.42
139.9	0.252	1.84	1.54	1.18	3.42

[a] Determined from the plot of I_s versus θ.
[b] Determined from the plot of $R(q)/q^2$ versus q^2.
[c] Estimated from q_m in the third row.

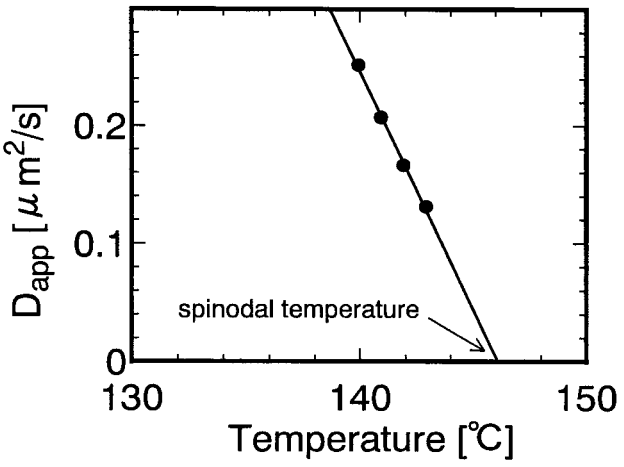

Figure 6 Temperature dependence of D_{app}.

proaches the binodal curve in this region of low polymer volume fraction.

Later Stage of Phase Separation

Figure 7 shows the light scattering profiles for the longer time. The experimental condition was the same as that in Figure 3, except for the experimental time. In contrast to the result in Figure 3, peaks of I_s shifted into smaller angle with time, accompanying with the increase of intensity. This means that the phase-separated structure grew in this time scale. Thus, it can be deduced that the

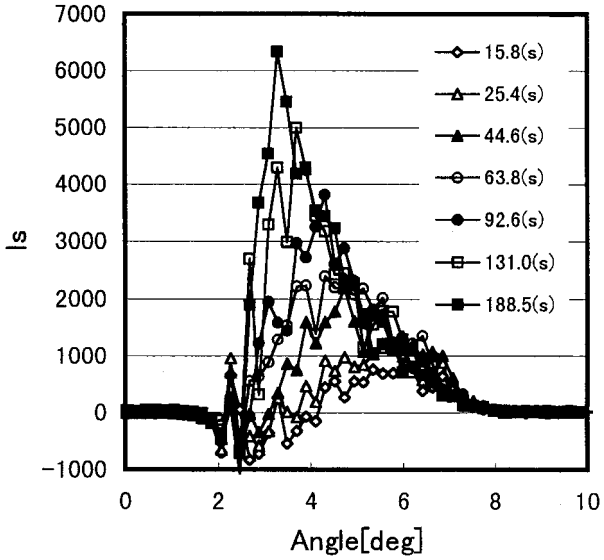

Figure 7 Light-scattering profiles for the longer time: quench temperature 140.9°C; polymer volume fraction 0.121.

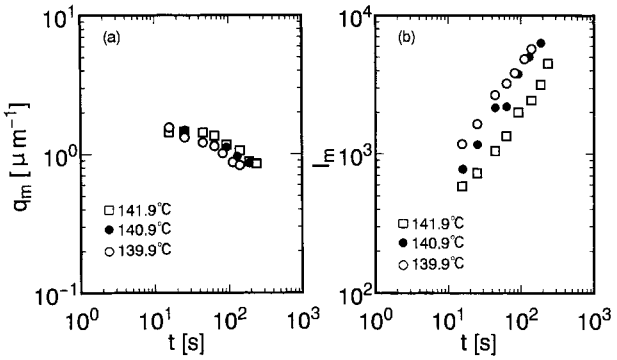

Figure 8 Logarithmic plots of q_m and I_m against time: (a) q_m versus time; (b) I_m versus time.

phase separation in this time scale was at the intermediate or late stage of SD.

The growth of the phase-separated structure in the later stage is characterized by scaling behaviors of q_m and the maximum scattered light intensity I_m as[48–50]:

$$q_m(t) \sim t^{-a} \tag{13}$$

$$I_m(t) \sim t^{b} \tag{14}$$

Logarithmic plots of q_m and I_m against t are shown in Figure 8(a) and (b) for the different quenches. The scaling exponents of a and b obtained for the data after 30 s are summarized in Table II. The ratio of b/a should be 3.0 for the late stage of SD; whereas, $b/a > 3.0$ is expected for the intermediate stage of SD.[48,49] The values of b/a shown in Table II are approximately equal to 3.0, suggesting that the phase separation after 30 s was at the late stage of SD.

The scaled structure factor $F(x, t)$ is defined as[48]:

$$F(x, t) = q_m^3(t) I_s(x, t) \qquad \text{with} \qquad x = q/q_m \tag{15}$$

Table II Scaling Exponents Obtained from Plots of Figure 8

Temperature (°C)	a	b	b/a
141.9	0.28	0.75	2.7
140.9	0.25	0.81	3.2
139.9	0.28	0.73	2.6

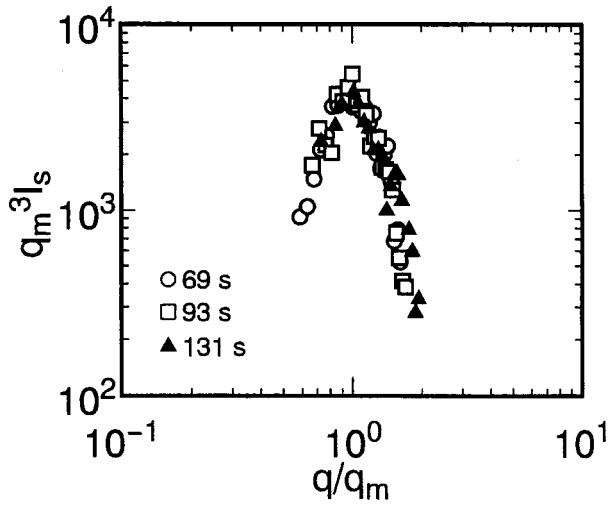

Figure 9 The scaled structure factors for various phase separation time: quench temperature 140.9°C; polymer volume fraction 0.121.

$F(x, t)$ is independent of t in the late stage of SD; whereas, time dependency appears in the intermediate stage of SD.[48] Figure 9 shows the plot of $q_m^3 I_s$ versus q/q_m for the data shown in Figure 7. The late-stage structure factor could be scaled into a universal time-independent form in agreement with the predictions of the dynamic scaling hypothesis.[51]

Figure 10 shows the optical micrographs of droplets formed from 10 wt % iPP sample. Because the experimental condition is the same as that in Figure 7, these structures brought about the light scattering shown in Figure 7. The droplets were clustered close together and coarsened with time.

The average droplet diameter determined from the optical micrograph is plotted with time in Figure 11. Figure 11(b) shows the logarithmic plot. The scaling exponent λ in the relation of droplet size $\propto t^{\lambda}$ was 0.316. Although the droplet growth mechanism in this system may be the coalescence-induced coalescence mechanism in the same manner as iPP/diphenyl ether system,[35] detailed discussion on the mechanism cannot be made only from the scaling exponent. When the structure is isolated and dispersed, the average interdomain distance D is estimated from Eq.

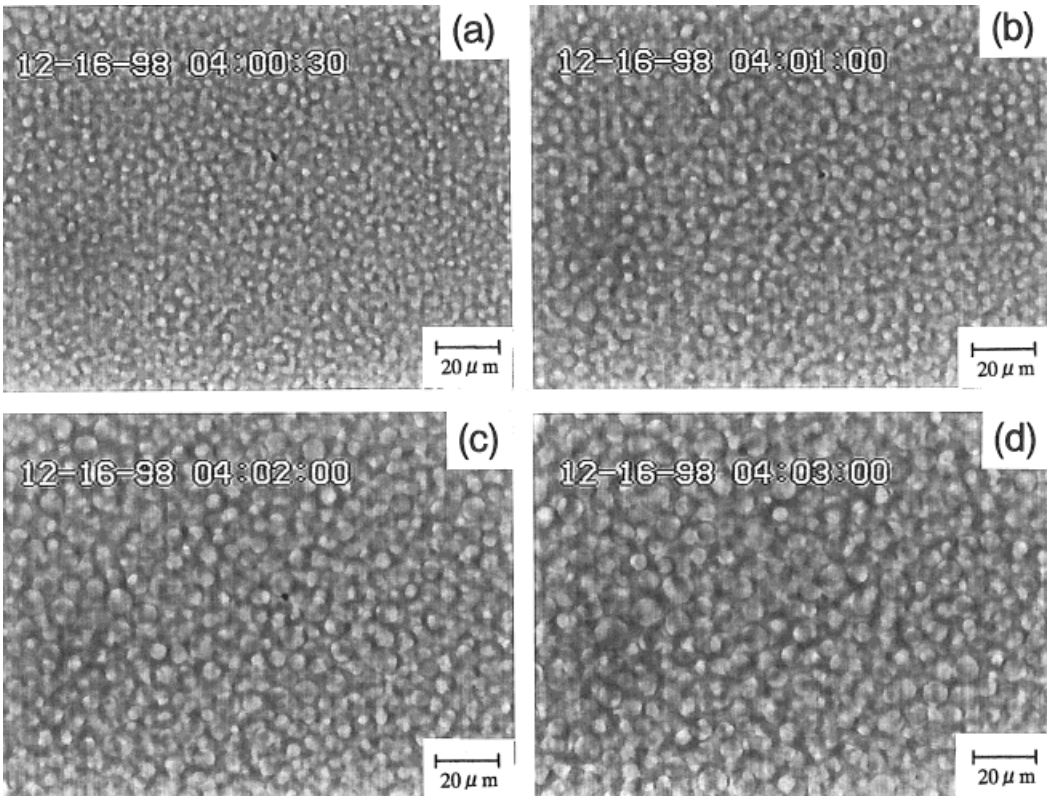

Figure 10 Optical micrographs of droplets: (a) t = 30 s; (b) t = 60 s; (c) t = 120 s; (d) t = 180 s; quench temperature 140.9°C; polymer volume fraction 0.121.

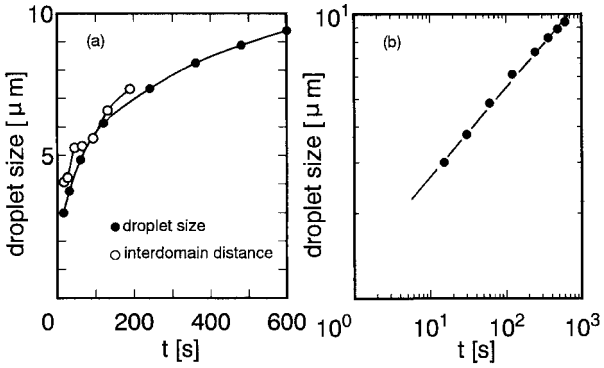

Figure 11 Average droplet diameter as a function of time: (a) linear plot; (●) average diameter; (○) average interdomain distance; (b) logarithmic plot; quench temperature 140.9°C; polymer volume fraction 0.121.

(10).[52,53] The interdomain distance D obtained from the light-scattering measurements is also plotted in Figure 11(a) as symbol ○. The interdomain distance roughly agreed with the droplet size. This may be because the droplet were clustered close together.

CONCLUSIONS

1. The phase diagram of iPP/MS system was clarified. The cloud points and the dynamic crystalline temperatures were determined by the optical microscope measurements and by DSC, respectively. The spinodal curve and the equilibrium melting points were calculated based on the Flory's theory.
2. The early stage of phase separation was studied by the light scattering. The phase separation mechanism was found to be the early stage of spinodal decomposition (SD). Characteristic properties of SD, such as D_{app}, q_m, τ_0 and Λ_m were determined according to the linear Cahn theory. The interphase periodic distance Λ_m ranged from 3 μm to 4 μm.
3. The growth of the phase-separated structure in the later stage was well characterized by scaling behaviors of q_m and I_m. From the obtained scaling exponents, it was suggested that the phase separation after 30 s was at the late stage of SD. The late-stage structure factor could be scaled into a universal time-independent form. The domain size obtained from the light-scattering measurements roughly agreed with the droplet size determined by the optical microscope.

REFERENCES

1. Mulder, M. Basic principles of membrane technology; Kluwer Academic Publishers: Dordrecht, 1996, p. 74.
2. van de Witte, P.; Dijkstra, P. J.; van den Berg, J. W. A.; Feijen J. J Membr Sci 1996, 117, 1–31.
3. Castro, A. J. Methods for making microporous products, US Patent 4,247,498, 1981.
4. Caneba, G. T.; Soong, D. S. Macromolecules 1985, 18, 2538–2545.
5. Caneba, G. T.; Soong, D. S. Macromolecules 1985, 18, 2545–2555.
6. Hiatt, W. C.; Vitzthum, G. H.; Wagener, K. B.; Gerlach, K.; Josefiak, C. ACS Symposium Series, 269, American Chemical Society: Washington, DC, 1985, pp. 229–244.
7. Aubert, J. H.; Clough, R. L. Polymer 1985, 26, 2047–2054.
8. Hikmet, R. M.; Callister, S.; Keller, A. Polymer 1988, 29, 1378–1388.
9. Tsai, F.-J.; Torkelson, J. M. Macromolecules 1990, 23, 775–784.
10. Lloyd, D. R.; Kinzer, K. E.; Tseng, H. S. J Membrane Sci 1990, 52, 239–261.
11. Lloyd, D. R.; Kim, S. S.; Kinzer, K. E. J Membrane Sci 1991, 64, 1–11.
12. Kim, S. S.; Lloyd, D. R. J Membr Sci 1991, 64, 13–29.
13. Lim, G. B. A.; Kim, S. S.; Ye, Q.; Wang, Y. E.; Lloyd, D. R. J Membr Sci 1991, 64, 31–40.
14. Alwattari, A. A.; Lloyd, D. R. J Membr Sci 1991, 64, 55–68.
15. Vandeweerdt, P.; Berghmans, H.; Tervoort, Y. Macromolecules 1991, 24, 3547–3552.
16. Vadalia, H. C.; Lee, H. K.; Myerson, A. S.; Levon, K. J Membr Sci 1994, 79, 37–50.
17. Mehta, R. H.; Madsen, D. A.; Kalika, D. S. J Membr Sci 1995, 107, 93–106.
18. Kim, J. J.; Hwang, J. R.; Kim, U. Y.; Kim, S. S. J Membr Sci 1995, 108, 25–36.
19. Cha, B. J.; Char, K.; Kim, J. J.; Kim, S. S.; Kim, C. K. J Membr Sci 1995, 108, 219–229.
20. Zryd, J. L.; Burghardt, W. R. J Appl Polym Sci 1995, 57, 1525–1537.
21. Caplan, M. R.; Chiang, C. Y.; Lloyd, D. R.; Yen, L. Y. J Membr Sci 1997, 130, 219–237.
22. Mehta, R. H.; Kalika, D. S. J Appl Polym Sci 1997, 66, 2347–2355.
23. Sun, H.; Kim, D. H.; Kitano, T.; Mah, S. I. Kobunshi Ronbunshu 1998, 55, 378–384.
24. Nojima, S.; Tsutsumi, K.; Nose, T. Polym J 1982, 14, 225–232.

25. Krishnamurthy, S.; Bansil, R. Phys Rev Lett 1983, 50, 2010–2013.
26. Cumming, A.; Wiltzius, P.; Bates, F. S. Phys Rev Lett 1990, 65, 863–866.
27. Aubert, J. H. Macromolecules 1990, 23, 1446–1452.
28. Lal, J.; Bansil, R. Macromolecules 1991, 24, 290–297.
29. Sato, H.; Kuwahara, N.; Kubota, K. Phys Rev E 1994, 50, 1752–1754.
30. Song, S.-W.; Torkelson, J. M. Macromolecules 1994, 27, 6389–6387.
31. Guo, H.-F.; Laxminarayan, A.; Caneba, G. T.; Solc, K. J Appl Polym Sci 1995, 55, 753–759.
32. Song, S.-W.; Torkelson, J. M. J Membr Sci 1995, 98, 209–222.
33. McGuire, K. S.; Laximinarayan, A.; Lloyd, D. R. Polymer 1995, 26, 4951–4960.
34. Siggia, E. D. Phys Rev A 1979, 20, 595–605.
35. McGuire, K. S.; Laxminarayan, A.; Martula, D. S.; Lloyd, D. R. J Colloid Interf Sci 1996, 182, 46–58.
36. Van Aartsen, J. J.; Smolders, C. A. Eur Polym J 1970, 6, 1105–1112.
37. Kuwahara, N.; Kubota, K. Phys Rev A 1992, 45, 7385–7314.
38. Cahn, J. W. J Chem Phys 1965, 42, 93–99.
39. McGuire, K. S.; Laxminarayan, A.; Lloyd, D. R. Polymer 1994, 20, 4404–4407.
40. Flory, P. J. Principles of Polymer Chemistry; Cornell University Press: Ithaca, NY, 1953.
41. Burghardt, W. R. Macromolecules 1989, 22, 2482–2486.
42. Clark, E. J.; Hoffman, J. D. Macromolecules 1984, 17, 878–885.
43. Kirshenbaum, I.; Wilchinsky, Z. W.; Groten, B. J Appl Polym Sci 1964, 8, 2723–2731.
44. Hashimoto, T.; Kumaki, J.; Kawai, H. Macromolecules 1983, 16, 641–648.
45. Sasaki, K.; Hashimoto, T. Macromolecules 1984, 17, 2818–2825.
46. Komatsu, M.; Inoue, T. J Polym Sci Polym Phys Ed 1986, 24, 303–311.
47. Otake, K.; Inomata, H.; Yagi, Y.; Konno, M.; Saito, S. Polym Comm 1989, 30, 203–205.
48. Hashimoto, T.; Itakura, M.; Haegawa, H. J Chem Phys 1986, 85, 6118–6128.
49. Hashimoto, T.; Itakura, M.; Shimidzu, N. J Chem Phys 1986, 85, 6773–6786.
50. Hashimoto, T.; Tanaka, M.; Jinnai, H. Polym Comm 1989, 30, 177–179.
51. Gunton, J. D.; San Miguel, M.; Sahni, P. S. Phase Transitions and Critical Phenomena, Academic Press, London, 1983, p. 267.
52. Hashimoto, T.; Sasaki, K.; Kawai, H. Macromolecules 1984, 17, 2812–2818.
53. Graham, P. D.; Pervan, A. J.; McHugh, A. J. Macromolecules 1997, 30, 1651–1655.